Supplementary Information for

Estrogen-dependent expression and function of secretogranin 2a in female-specific peptidergic neurons

Thomas Fleming, Masaya Tachizawa, Yuji Nishiike, Ai Koiwa, Yuki Homan, and Kataaki Okubo*

*Corresponding author: Kataaki Okubo; Email: a-okubo@g.ecc.u-tokyo.ac.jp

This PDF file includes:

Table S1 to S3
Figure S1 to S8

Table S1. Abbreviations of brain nuclei.

abbreviation	full name	location
Ci	interpeduncular corpus	brain stem
CP	central posterior nucleus	thalamus
Dl	lateral nucleus of the dorsal telencephalic area	dorsal telencephalon
DP	dorsal posterior nucleus	thalamus
DT	dorsal tegmental nucleus	midbrain tegmentum
Hd	dorsal habenula	habenula
IR	inferior rectus of the oculomotor nerve nucleus	midbrain tegmentum
is	isthmus nucleus	brain stem
MR	medial rectus of the oculomotor nerve nucleus	midbrain tegmentum
NAT	anterior tuberal nucleus	hypothalamus
NPPv	posterior periventricular nucleus	hypothalamus
NPT	posterior tuberal nucleus	hypothalamus
NRL	lateral recess nucleus	hypothalamus
NRP	posterior recess nucleus	hypothalamus
NVm	trigeminal motor nucleus	brain stem
NVT	ventral tuberal nucleus	hypothalamus
Pbl	basal lateral preoptic nucleus	preoptic area
PMg	gigantocellular portion of the magnocellular preoptic nucleus	preoptic area
PMm	magnocellular portion of the magnocellular preoptic nucleus	preoptic area
PMp	parvocellular portion of the magnocellular preoptic nucleus	preoptic area
PPa	anterior parvocellular preoptic nucleus	preoptic area
PPp	posterior parvocellular preoptic nucleus	preoptic area
ra	raphe nucleus	brain stem
TL	lateral tuberal nucleus	hypothalamus
TN	terminal nerve ganglion	ventral telencephalon
VL	ventrolateral nucleus	thalamus
Vl	lateral nucleus of the ventral telencephalic area	ventral telencephalon
VM	ventromedial nucleus	thalamus
Vp	posterior nucleus of the ventral telencephalic area	ventral telencephalon
Vs	supracommissural nucleus of the ventral telencephalic area	ventral telencephalon
Vv	ventral nucleus of the ventral telencephalic area	ventral telencephalon

Table S2. Species names and GenBank accession numbers of the protein sequences used in this study.

protein	species	accession number
SCG2	human (*Homo sapiens*)	NP_003460
SCG2	bovine (*Bos taurus*)	NP_776601
SCG2	mouse (*Mus musculus*)	NP_033155
SCG2	rat (*Rattus norvegicus*)	NP_073160
Scg2 (predicted)	chicken (*Gallus gallus*)	XP_040535213
Scg2	*Xenopus* (*Xenopus tropicalis*)	NP_001072311
Scg2a (predicted)	tilapia (*Oreochromis aureus*)	XP_039478438
Scg2a (predicted)	zebrafish (*Danio rerio*)	XP_009290228
Scg2a (predicted)	cavefish (*Astyanax mexicanus*)	XP_007237528
Scg2b (predicted)	tilapia (*Oreochromis aureus*)	XP_031611738
Scg2b	zebrafish (*Danio rerio*)	NP_001071216
Scg2b (predicted)	cavefish (*Astyanax mexicanus*)	XP_022534954
CHGA	human (*Homo sapiens*)	NP_001266
CHGB	human (*Homo sapiens*)	NP_001810

Table S3. Primers and probes used in this study.

	target	direction	purpose	sequence (5′ to 3′)
primer	*scg2a*	forward	real-time PCR	CGCGCCAAATAATTACGAAAG
primer	*scg2a*	reverse	real-time PCR	CAGCAGAAGCGAACACAAGAAG
primer	*actb*	forward	real-time PCR	CCCCACCCAAAGTTTAG
primer	*actb*	reverse	real-time PCR	CAACGATGGAGGGAAAGACA
primer	*eef1a*	forward	real-time PCR	AGAAGGAAGCCGCTGAGATG
primer	*eef1a*	reverse	real-time PCR	AGAGCGATGTCGATGGTGATAC
primer	*scg2a*	forward	genotyping (gDNA PCR)	AAGACAGGATAAGAGTGAAGAGCT
primer	*scg2a*	reverse	genotyping (gDNA PCR)	CAGCATCATCTGCATTATTAGACC
primer	*scg2a*	forward	genotyping (CS)	AGAGACCAGGAACAAACAGAGG
primer	*scg2a*	forward	genotyping (HRM)	GAGGAAGGTGAGGATGACAGGG
primer	*scg2a*	reverse	genotyping (HRM)	TCCAGCTCGTCAAACACAGACT
probe	*scg2a*	forward	genotyping (HRM)	CGCACCAAAGAAAACGTGGAGGAG AAGTAC
primer	*esr1*	forward	genotyping (gDNA PCR)	TCCGGTGGAAAACACAAGTCTG
primer	*esr1*	reverse	genotyping (gDNA PCR)	TTTATCTGCACCCTTGCGGAGT
primer	*esr1*	forward	genotyping (CS)	AGGGAGGACCAGTGCGGCT
primer	*esr2b*	forward	genotyping (gDNA PCR)	AATAATGACCCGTTAACGTTGCT
primer	*esr2b*	reverse	genotyping (gDNA PCR)	TCAATTTTCAGTCACAAATGCAC
primer	*esr2b*	forward	genotyping (CS)	TCCAGCTCCAAGAGGTAGATG
primer	*esr2b*	forward	genotyping (HRM)	GCAGCCATGACTATGGGAAC
primer	*esr2b*	reverse	genotyping (HRM)	GACTATGGGAGGGCCAAAAG
probe	*esr2b*	forward	genotyping (HRM)	GGGCCTGGACCGTTGACCTTCTATA GTCC

gDNA PCR, PCR on genomic DNA; CS, cycle sequence; HRM, high resolution melt analysis.

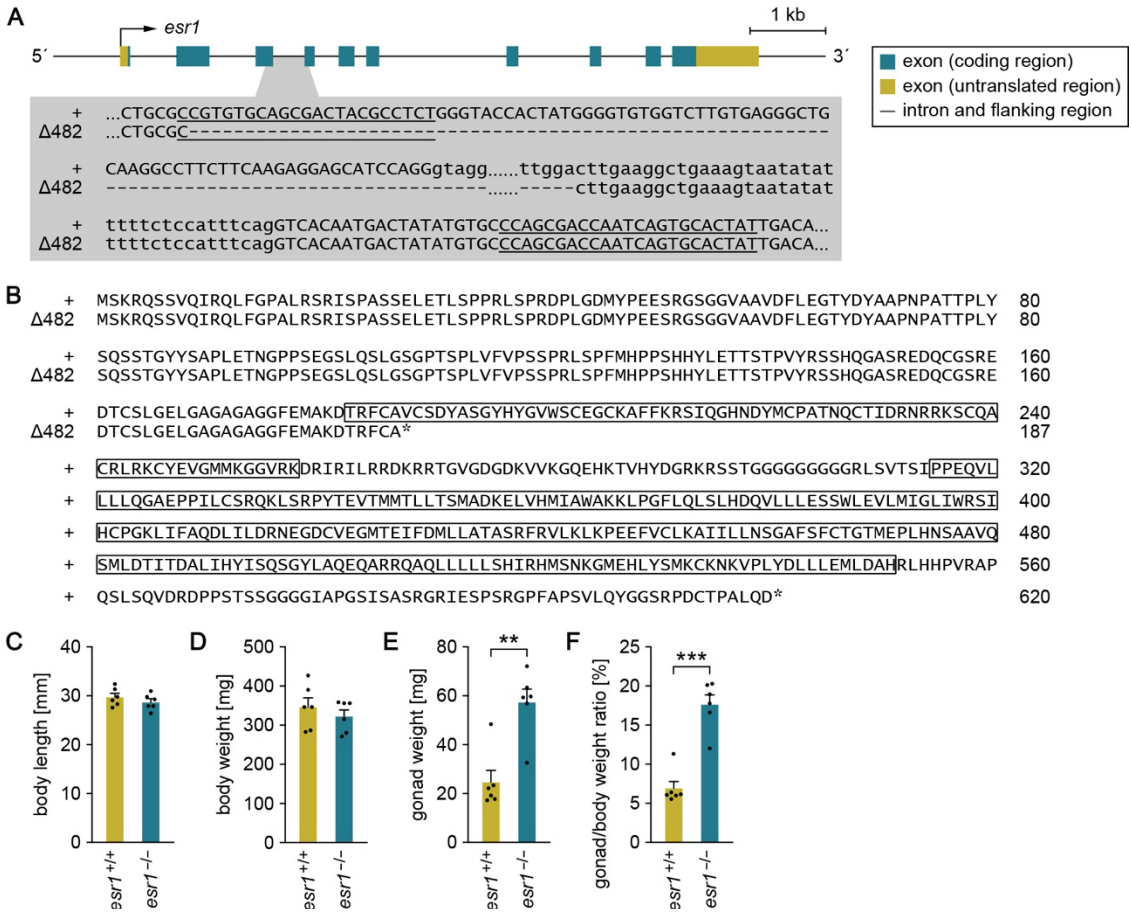

Fig. S1. Generation and characterization of *esr1*-deficient medaka. An *esr1* knockout medaka line was generated using CRISPR/Cas9-mediated genome editing. (A) The gene structure of medaka *esr1* is shown with the location of the two CRISPR target sites, which are enlarged to depict the nucleotide sequences of the wild-type (+) and targeted (Δ482) alleles. Exon and intron sequences are given in uppercase and lowercase letters, respectively. The sequences targeted by the CRISPR RNAs are underlined and deleted nucleotides are represented by dashes. (B) Comparison of the deduced amino acid sequences of the wild-type and Δ482 alleles. The DNA- and ligand-binding domains are indicated by the first and second boxes, respectively. Asterisks indicate stop codons. (C–F) Body length (C), body weight (D), gonad weight (E), and gonad/body weight ratio (F) of adult $esr1^{+/+}$ and $esr1^{-/-}$ females (n = 6 for each genotype). Statistical differences were assessed by unpaired *t*-test (C–F). $^{**}p < 0.01$; $^{***}p < 0.001$.

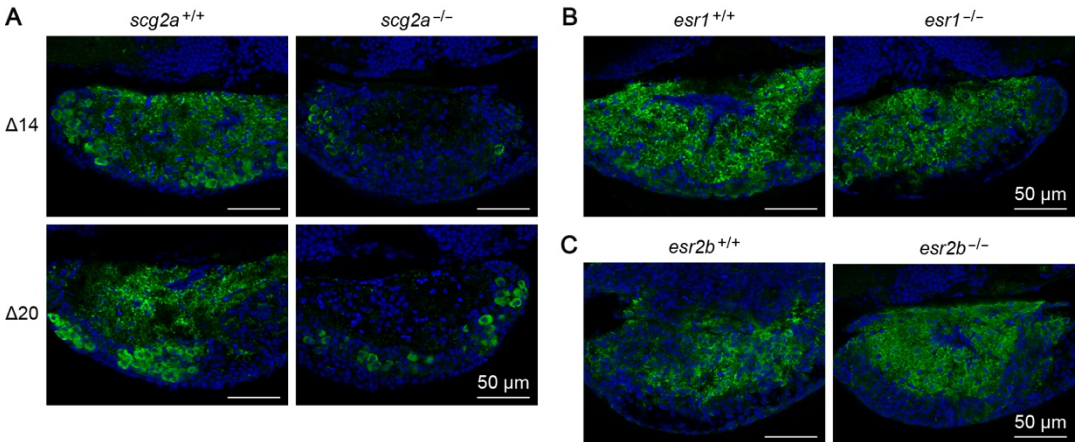

Fig. S2. Localization and estrogen regulation of SNa in the pituitary. (A) Representative micrographs of the pituitary from *scg2a*$^{+/+}$ and *scg2a*$^{-/-}$ females of the Δ14 and Δ20 lines (see Fig. S3) showing the localization of SNa immunofluorescence (green) in the pituitary. (B, C) Representative micrographs of the pituitary from *esr1*$^{+/+}$ and *esr1*$^{-/-}$ (B) and *esr2b*$^{+/+}$ and *esr2b*$^{-/-}$ (C) females showing no apparent effect on SNa immunofluorescence (green) in the pituitary from the loss of these receptors. Cell nuclei are shown in blue. Scale bars in all panels represent 50 μm.

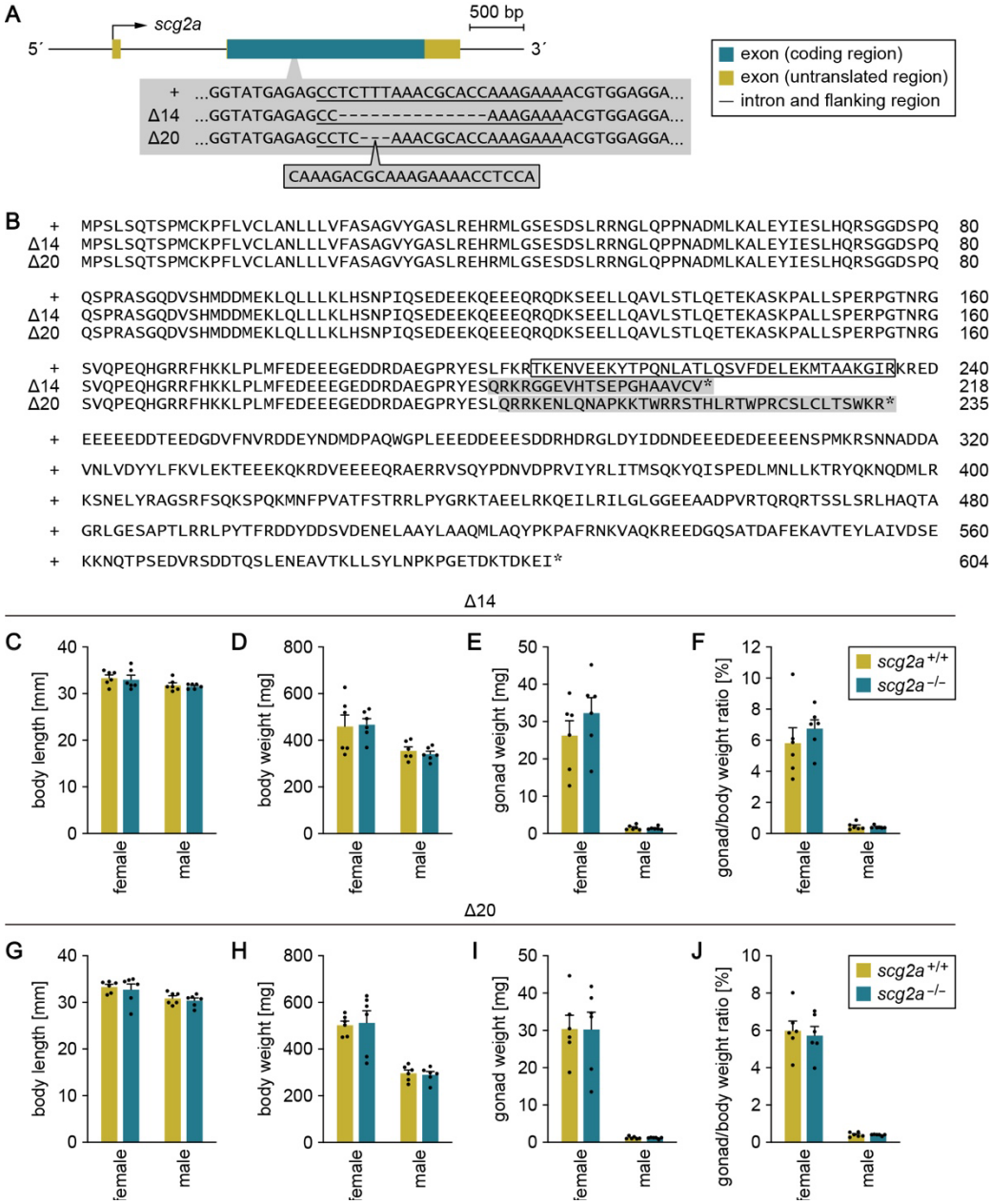

Fig. S3. Generation and characterization of *scg2a*-deficient medaka. Two independent lines of *scg2a* knockout medaka (Δ14 and Δ20) were generated using CRISPR/Cas9-mediated genome editing. (A) The gene structure of medaka *scg2a* is shown with the location of the CRISPR target site, which is enlarged to depict the nucleotide sequences of the wild-type (+) and targeted (Δ14 and Δ20) alleles. The sequence targeted by the CRISPR RNA is underlined and deleted nucleotides are represented by dashes. (B) Comparison of the deduced amino acid sequences of the wild-type, Δ14, and Δ20 alleles. The mature SNa polypeptide region is indicated by a box. Altered sequence caused by a frameshift is shaded in gray. Asterisks indicate stop codons. (C–F) Body length (C), body weight (D), gonad weight (E), and gonad/body weight ratio (F) of adult *scg2a*$^{+/+}$ and *scg2a*$^{-/-}$ females and males of the Δ14 line (n = 6 for each sex and genotype). (G–J) Body length (G), body weight (H), gonad weight (I), and gonad/body weight ratio (J) of adult *scg2a*$^{+/+}$ and *scg2a*$^{-/-}$ females and males of the Δ20 line (n = 6 for each sex and genotype). Statistical differences were assessed by unpaired *t*-test with Bonferroni-Dunn correction (C–J).

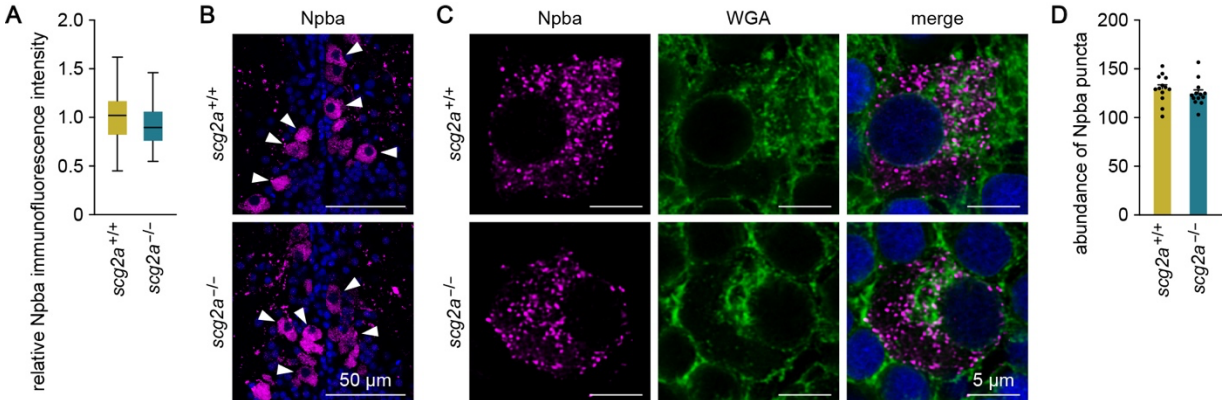

Fig. S4. Scg2a is not involved in neuropeptide packaging to secretory granules in FeSP neurons—Δ20 line. (A) Relative intensity of Npba immunofluorescence in FeSP neurons of *scg2a*$^{+/+}$ (n = 78 neurons) and *scg2a*$^{-/-}$ (n = 66 neurons) females. Mean intensity in *scg2a*$^{+/+}$ FeSP neurons was arbitrarily set to 1. (B) Representative micrographs showing Npba immunofluorescence (magenta) in FeSP neurons (arrowheads) of *scg2a*$^{+/+}$ and *scg2a*$^{-/-}$ females. Cell nuclei are shown in blue. Scale bars represent 50 µm. (C) Representative micrographs showing the distribution of Npba puncta (left panels; magenta) in *scg2a*$^{+/+}$ and *scg2a*$^{-/-}$ FeSP neurons, counterstained with wheat germ agglutinin (WGA) (middle panels; green). Right panels show merged images with nuclear counterstaining (blue). Scale bars represent 5 µm. (D) Abundance of Npba puncta in FeSP neurons of *scg2a*$^{+/+}$ and *scg2a*$^{-/-}$ females (n = 13 neurons for each genotype). Statistical differences were assessed by unpaired *t*-test (A, D).

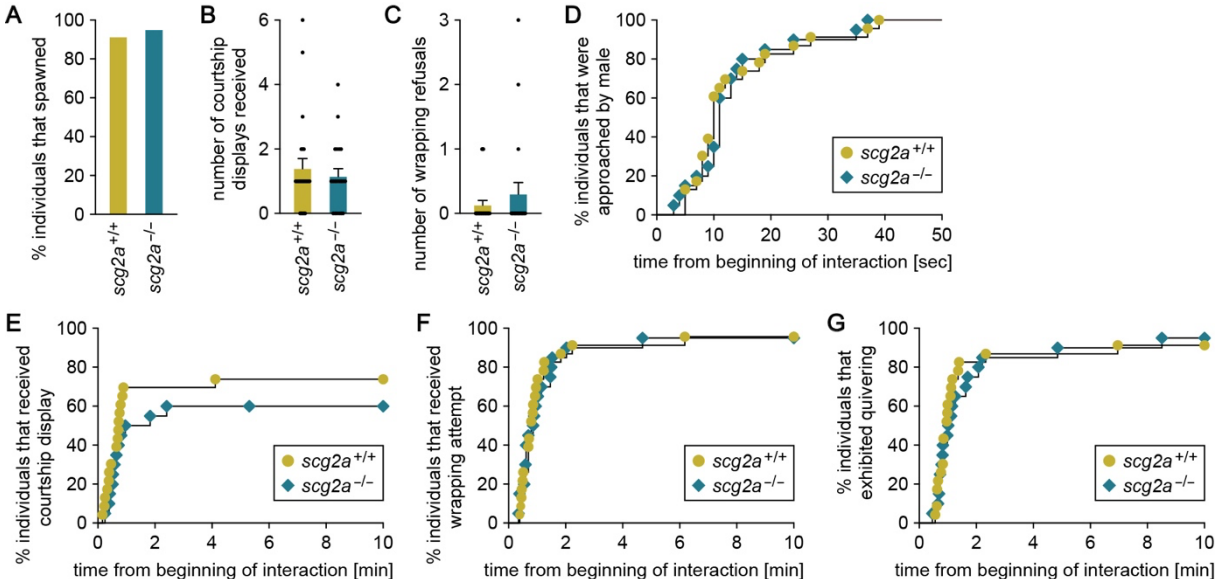

Fig. S5. *scg2a*-deficient female medaka show no alterations in mating behavior—Δ20 line. *scg2a*$^{+/+}$ (n = 23) and *scg2a*$^{-/-}$ (n = 20) females of the Δ20 line were tested for mating behavior. (A) Percentage of individuals that spawned within the test period (10 min). (B, C) Number of courtship displays received (B) and wrapping refusals (C). (D–G) Latency from the beginning of interaction to the first approach (D), first courtship display (E), first wrapping attempt (F), and quivering (G). Statistical differences were assessed by Fisher's exact test (A), unpaired *t*-test (B), unpaired *t*-test with Welch's correction (C), and Gehan-Breslow-Wilcoxon test (D–G).

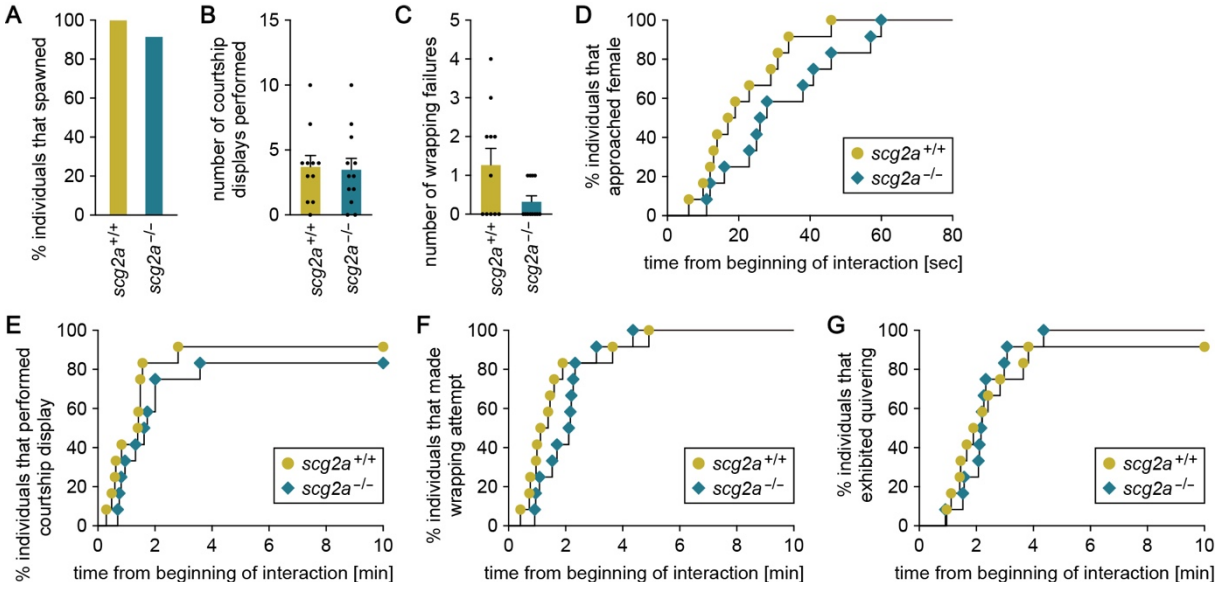

Fig. S6. *scg2a*-deficient male medaka show no alterations in mating behavior—Δ14 line. *scg2a*$^{+/+}$ and *scg2a*$^{-/-}$ males (n = 12 for each genotype) of the Δ14 line were tested for mating behavior. (A) Percentage of individuals that spawned within the test period (10 min). (B, C) Number of courtship displays performed (B) and wrapping refusals by the female (C). (D–G) Latency from the beginning of interaction to the first approach (D), first courtship display (E), first wrapping attempt (F), and quivering (G). Statistical differences were assessed by Fisher's exact test (A), unpaired *t*-test (B), unpaired *t*-test with Welch's correction (C), and Gehan-Breslow-Wilcoxon test (D–G).

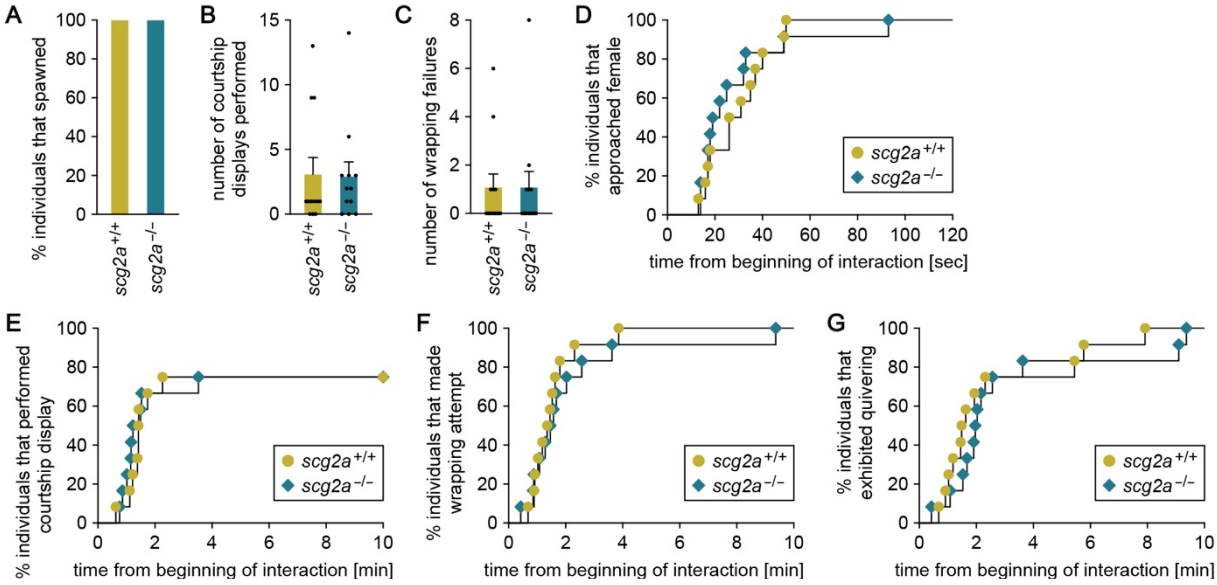

Fig. S7. *scg2a*-deficient male medaka show no alterations in mating behavior—Δ20 line. *scg2a*$^{+/+}$ and *scg2a*$^{-/-}$ males (n = 12 for each genotype) of the Δ20 line were tested for mating behavior. (A) Percentage of individuals that spawned within the test period (10 min). (B, C) Number of courtship displays performed (B) and wrapping refusals by the female (C). (D–G) Latency from the beginning of interaction to the first approach (D), first courtship display (E), first wrapping attempt (F), and quivering (G). Statistical differences were assessed by Fisher's exact test (A), unpaired *t*-test (B, C), and Gehan-Breslow-Wilcoxon test (D–G).

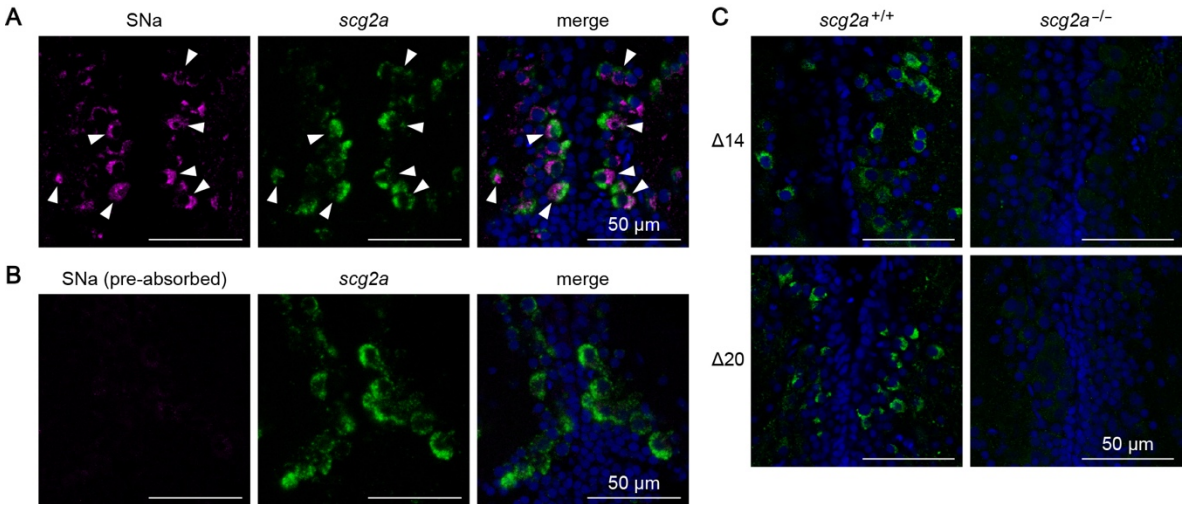

Fig. S8. Validation of the anti-SNa antibody. All micrographs shown are representative images of the PMm/PMg of females. (A) Co-localization of immunofluorescence obtained with the anti-SNa antibody (left panel; magenta) and *scg2a* transcript (middle panel; green); right panel shows the merged image with nuclear counterstaining (blue). Arrowheads indicate representative neurons labeled with both SNa immunofluorescence and *scg2a* transcript. (B) Loss of immunofluorescence (left panel; magenta) in neurons expressing the *scg2a* transcript (middle panel; green) after pre-absorption of the anti-SNa antibody with the SNa polypeptide; right panel shows the merged image with nuclear counterstaining (blue). (C) Loss of neurons immunolabeled with the anti-SNa antibody (green) in *scg2a*$^{-/-}$ fish from both Δ14 and Δ20 lines (compare right panels with left panels). Cell nuclei are shown in blue. Scale bars in all panels represent 50 µm.